Carbohydrate Polymers 95 (2013) 252–261

Contents lists available at SciVerse ScienceDirect

Carbohydrate Polymers

journal homepage: www.elsevier.com/locate/carbpol

Uniquely different PVA-xanthan gum irradiated membranes as transdermal diltiazem delivery device

Tridib Bhunia, Arindam Giri, Tanbir Nasim, Dipankar Chattopadhyay, Abhijit Bandyopadhyay*

Department of Polymer Science and Technology, University of Calcutta, 92, A.P.C. Road, Calcutta 700009, India

ARTICLE INFO

Article history:
Received 6 November 2012
Received in revised form
26 December 2012
Accepted 21 February 2013
Available online 4 March 2013

Keywords:
PVA
Molecular weight
Xanthan gum
Irradiation
Drug delivery

ABSTRACT

This paper reports interesting differences between physical and mechanical properties of various membranes prepared from high and low molecular weight poly (vinyl alcohol) (PVA) and xanthan gum (XG) blends irradiated under low dose electron beam. The membranes were designed for sustained delivery of diltiazem hydrochloride through skin. Electron beam irradiation produced crosslinks and turned PVA into crystalline phase from its amorphous organization in the unirradiated state. PVA crystals were fibrillar at low XG content (1 wt.%) when the molecular weight was high while similar orientation at higher XG content (5 wt.%) when the molecular weight was low. Low molecular weight PVA–XG membranes showed equivalent physical properties under dry condition but wet-mechanical properties were superior for high molecular weight PVA–XG hybrids. Both of them showed slow and sustained diltiazem release but the later induced slightly slower release despite low drug encapsulation efficiency due to its better wet mechanical strength.

1. Introduction

Synthetic polymers are highly effective in formulating various hydrogels as biomedical grafts (Coombes & Meikle, 1994; Tanzi et al., 1985), implants (Middleton & Tipton, 2000) and transdermal patches (Gao, Liang, Liu, & Xiao, 2009; Kotiyan, Vavia, Bharadwaj, Sabarwal, & Majali, 2002) since they provide excellent combination of physical and mechanical properties (Pakhomov, Korsukov, Shablygin, & Novak, 1984). But recent environmental concern has attracted increasing interest toward biodegradable (natural) polymers for similar applications (Chandra & Rustgi, 1998; Huang, Qi, feng, Su, & He, 2011). Tiny grafts or implants can be easily made using natural polymers but it is highly difficult to formulate drug delivery patches using them due to their exceedingly poor cohesive strength (Tang, Sun, Li, Wu, & Lin, 2009). Thus, what now has been realized that use of synthetic polymers is inevitable and under such circumstances blending between natural and synthetic polymers is the most viable option to undermine deleterious environmental impact (Singh & Sharma, 2010; Zhao et al., 2003). Upholding this blending theory, several blend compositions involving PVA and other synthetic polymers have already been exploited (Lee, Kim, & Kim, 1996; Nishino, Kani, Gotoh, & Nakamae, 2002; Yoon, Park, & Byun, 2012).

PVA is a unique synthetic polymer having great combination of strength, flexibility, biocompatibility, air permeability and water absorption properties (Deng & Hagg, 2010; Nuttelman, Henry, & Anseth, 2002; Xiao & Zhou, 2003; Yang, Smolen, & Peppas, 1981; Zhang, Yuan, & Wang, 2007). It is commercially available in several molecular weights and hydrolysis grades (Finch, 1973). The polymer has already established its identity as potentially excellent contact lens (Peterson, Wolffsohn, Nick, Winterton, & Lally, 2006), articular cartilage (Stammen, Williams, Ku, & Guldberg, 2001), artificial muscle (Wang, Oh, & Lee, 2010) and vascular cell culturing hydrogel (Jiang, Liu, & Feng, 2011). But all grades of PVA are not biodegradable. Also, not many literatures are available which explores performance differences between various PVAs on several biomedical devices developed so far. This last issue has been deliberately raised because huge contrast in physical and mechanical properties has already been observed by our group once we have shifted down from the most familiar high molecular weight grade PVA (PVA_H, Mn 115,000) to its oligomeric grade (PVA_L, Mn 14,000) (Bhunia, Bhowmik, Chattopadhyay, & Bandyopadhyay, 2012; Bhunia, Chattopadhyay, & Bandyopadhyay, 2011). These differences had impacted their performance quite significantly. In this connection, the present article features some unique behaviors of these two biodegradable PVAs toward XG in a blend composition meant for transdermal drug delivery application.

* Corresponding author. Tel.: +91 033 235013976996/6387/8386x288.
E-mail addresses: abpoly@caluniv.ac.in, abhijitbandyopadhyay@yahoo.co.in (A. Bandyopadhyay).

0144-8617/$ – see front matter © 2013 Elsevier Ltd. All rights reserved.
http://dx.doi.org/10.1016/j.carbpol.2013.02.043

Table 1
Sample compositions, FTIR peak intensity ratio, crystallite size, % crystallinity, DSC melting enthalpy, drug diffusion coefficient (k) and release exponent (n) values of different PVA–XG hybrid membranes.

Sample designation	PVA% (w/v)	XG (wt.%) w.r.t. PVA	FTIR peak intensity ratio ($I_{1140/850}$)	XRD crystal size (nm)	Peak position (2θ)	% Crystallinity	DSC melting peak position (°C)	Melting enthalpy (mJ/g)	k	n
$PVA_{H/0}$	10	0	0.78	19.53	19.65	4.069	226.6	723	2.17	0.91
$PVA_{H/1}$	10	1.0	1.38	27.04	19.35	2.711	225.8	308	1.39	1.21
$PVA_{H/3}$	10	3.0	–	22.51	19.45	3.362	–	–	–	–
$PVA_{H/5}$	10	5.0	–	20.53	19.55	3.458	226.3	544	–	–
$PVA_{L/0}$	10	0	0.81	19.53	19.65	4.069	226.6	638	2.37	0.92
$PVA_{L/1}$	10	1.0	–	20.39	19.64	3.943	226.1	372	–	
$PVA_{L/3}$	10	3.0	–	21.62	19.61	3.923	–	–	–	–
$PVA_{L/5}$	10	5.0	1.23	22.68	19.56	3.911	226.0	298	1.54	1.11

Transdermal patches are miraculous discovery in drug therapy where drugs with shorter half life and severe side effects are delivered in controlled way through skin (Mahmarian et al., 1994). Similar patches for nicotine delivery (Davaran, Rashidi, Khandaghi, & Hashemi, 2005), testosterone delivery (Raynaud, Aumonier, Gualano, Betea, & Beckers, 2008) etc. are already commercialized. Diltiazem hydrochloride or diltiazem is an important multipurpose drug used for treating patients suffering from both chest pain (angina pectoris) and anal fissure (Prisant & Elliott, 2003; Puche, Garcia-Coret, Villalba, Mahmoud, & Roig, 2010). It has low half life of only 3–4.5 h and is available as 30 mg or higher dose tablets. Intravenous (IV) formulations are also available for emergency. Required dose for an adult individual is 180 mg/day. Its premium side effects include tremendously low blood pressure and heart beat. Not much work on controlled delivery of this important drug has been reported so far. For skin delivery of diltiazem or any other drug, the intended device requires amazing combination of high strength, viscosity, flexibility, biodegradability and encapsulation efficiency with controlled water absorption. Both PVA_H and PVA_L satisfy many of these properties but unfortunately due to uncontrolled moisture absorption, accurate property prediction becomes highly difficult. In our earlier investigation we have added different nanomaterials into PVA to achieve better property control (Bhunia, Giri, Nasim, Chattopadhyay, & Bandyopadhyay, 2013; Bhunia, Goswami, Chattopadhyay, & Bandyopadhyay, 2011). In this article edible XG has been added and the blends were irradiated under electron beam to achieve the same. XG is a familiar thickener as well as stabilizer used in several food items (Garcia-Ochoa, santos, Casas, & Gomez, 2000; Izawa, Kaneko, & Kadokawa, 2009). It is far more viscous and hygroscopic than PVA (Bhunia, Chattopadhyay, et al., 2011; Sereno, Hill, & Mitchell, 2007) and contains interactive hydroxyl groups. It is highly crystalline and has very low water solubility. Different PVA-XG blends were irradiated under low dose of 5 kGy to prevent excessive chain degradation. Low dose irradiation usually promotes crosslinking in polymers and thus expected to offer better property control than else. It is more advantageous than chemical crosslinking since contamination (external crosslinker) can be avoided (Barash et al., 2010). Also, it would not degrade the entrapped drug molecules as well. In this article, different physical and mechanical properties related to diltiazem encapsulation and release from these irradiated blends has been investigated both under dry and wet conditions and a comparative account has been presented with possible reasoning.

2. Experimental

2.1. Materials

PVA of widely different number average molecular weights, 1.15×10^5 and 1.4×10^4, designated as PVA_H and PVA_L, with narrow molecular weight distribution (polydispersity index = 1.42) were purchased from Loba Chemie, Mumbai, India. XG was also purchased from Loba Chemie, Mumbai, India. Diltiazem hydrochloride, molecular weight 450.98, was a gift sample received from Ranbaxy Int., Gurgaon, Haryana, India.

2.2. Membrane preparation

At first XG was mixed with PVA in different weight proportion. Then standard 10% (w/v) PVA solution premixed with XG was prepared by dissolving PVA-XG mixture in hot distilled water under vigorous stirring. Then the formulated aqueous gel was placed into polyethylene bags (the thickness of the bags were 5 mm) and was irradiated at 5 kGy dose under high energy electron beam. The parameters of the accelerator were: electron energy 1.45 MeV; electron beam current 4 mA; scanner width 90 cm and conveyor speed 3.6 m min^{-1}. The post irradiated gels were cast on plane Teflon sheets for spontaneous drying at room temperature. The average thickness of the membranes was maintained at 0.25 cm during casting. Hybrid membranes that showed excellent physico-mechanical properties from each series were further prepared with diltiazem hydrochloride. In those cases, known weight of diltiazem (1 mg) was added to PVA and sonicated for 30 min. Detail of sample composition has been reported in Table 1.

2.3. Characterization of PVA–XG hybrid membranes

Atomic force microscope from Digital Instruments (Nanoscope III) was used to investigate the morphological aspects of the hybrid membranes. Topographic phase images were recorded in Force modulated taping mode with set point ratio of 0.9 using rotated tapping etched silicon probe (RTESP) tip having spring constant of 40 N/m. The cantilever was oscillated at a resonance frequency of 280 kHz.

Fourier transform infrared (FTIR) spectra of all the membranes was recorded using a JASCO FTIR machine at room temperature within the spectral range of 400–4000 cm^{-1} at a resolution of 4 cm^{-1} in dispersive mode. An average of 120 scans for each sample was reported for analysis.

Wide angle X-ray diffraction (XRD) behavior of hydrogel membranes was studied in a X'pert PRO MRD X-ray diffractometer (PANalytical, The Netherlands) at room temperature (27 ± 2 °C). The membranes were scanned between angles 10° and 35°. Spectral data corresponding to both dry and wet membranes were taken and are reproduced for analysis.

A Perkin-Elmer differential scanning calorimeter (DSC 7, Diamond) calibrated with indium was used to measure the melting characteristics of the hybrids. 5–6 mg samples were taken in a copper pan and scanned from 30 °C to 250 °C under nitrogen at the heating rate of 10 °C/min.

Tensile stress-strain properties (tensile strength, modulus and elongation at break) of the membranes were studied in a Lloyd UTM, USA at room temperature (27 ± 2 °C). The membranes were cut in

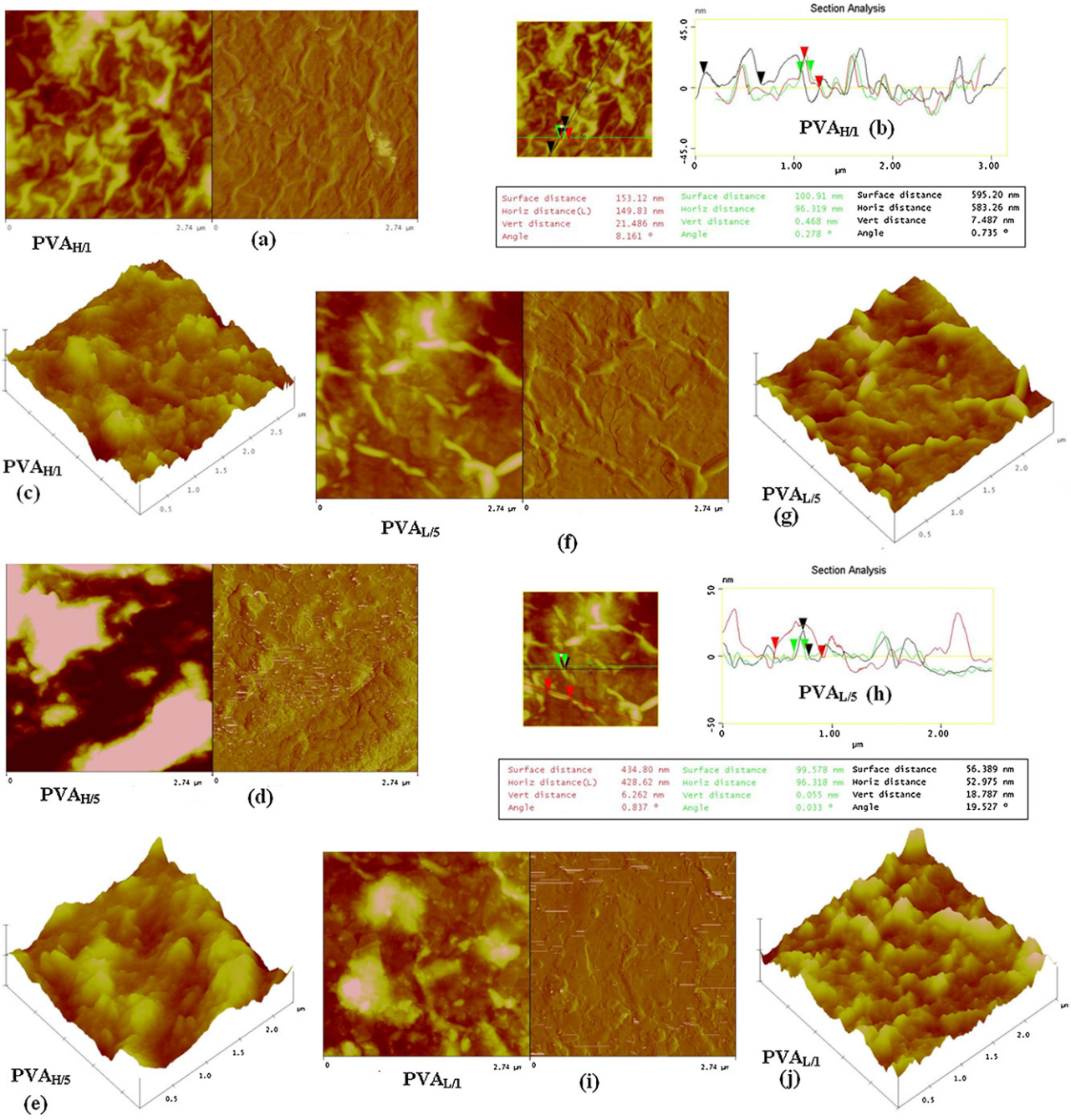

Fig. 1. AFM phase, height, 3D and section analysis of different PVA–XG hybrid membranes.

dimensions as per ASTM Die C and pulled at a rate of 10 mm/min. An average of five test results has been reported for analysis.

Swelling of hydrogel membranes was studied by putting samples in distilled water at room temperature ($27 \pm 2\,^{\circ}C$). After stipulated time interval, the samples were taken out of the water, gently wiped in tissue paper to soak surface water and then weighed in an electronic balance (MK-20E, readability 0.1 mg Adair Dutt, India). The swelling ratio was calculated by dividing swelled weight (S) by dry weight (S_0) of the membranes. The experiment was carried out till the samples attained equilibrium. Tensile measurements with fully swollen membranes were repeated using same instrument to compare their wet mechanical properties. De-swelling experiment was done by periodically recording the decreasing weight of the fully swollen membranes in ambient air ($27\,^{\circ}C$, RH: 85) till constant value was achieved.

2.4. Drug encapsulation efficiency (DEE) and transdermal diltiazem release analysis

DEE was analyzed by immersing the best membranes from each series into saturated diltiazem solution and allowed the drug to diffuse inside the membranes (sorption). Reduced drug concentration in the solution was monitored through UV spectroscopic measurement at 236 nm (Perkin-Elmer Lambda 25 1.27) and comparing that with a standard calibration curve. A plot was generated with % drug absorbed against time interval to demonstrate DEE for each hybrid membrane.

Transdermal release of diltiazem was analyzed in a Franz diffusion cell. Detailed description of the experiment has been reported in our earlier publication (Bhunia, Goswami, et al., 2011; Bhunia et al., 2012).

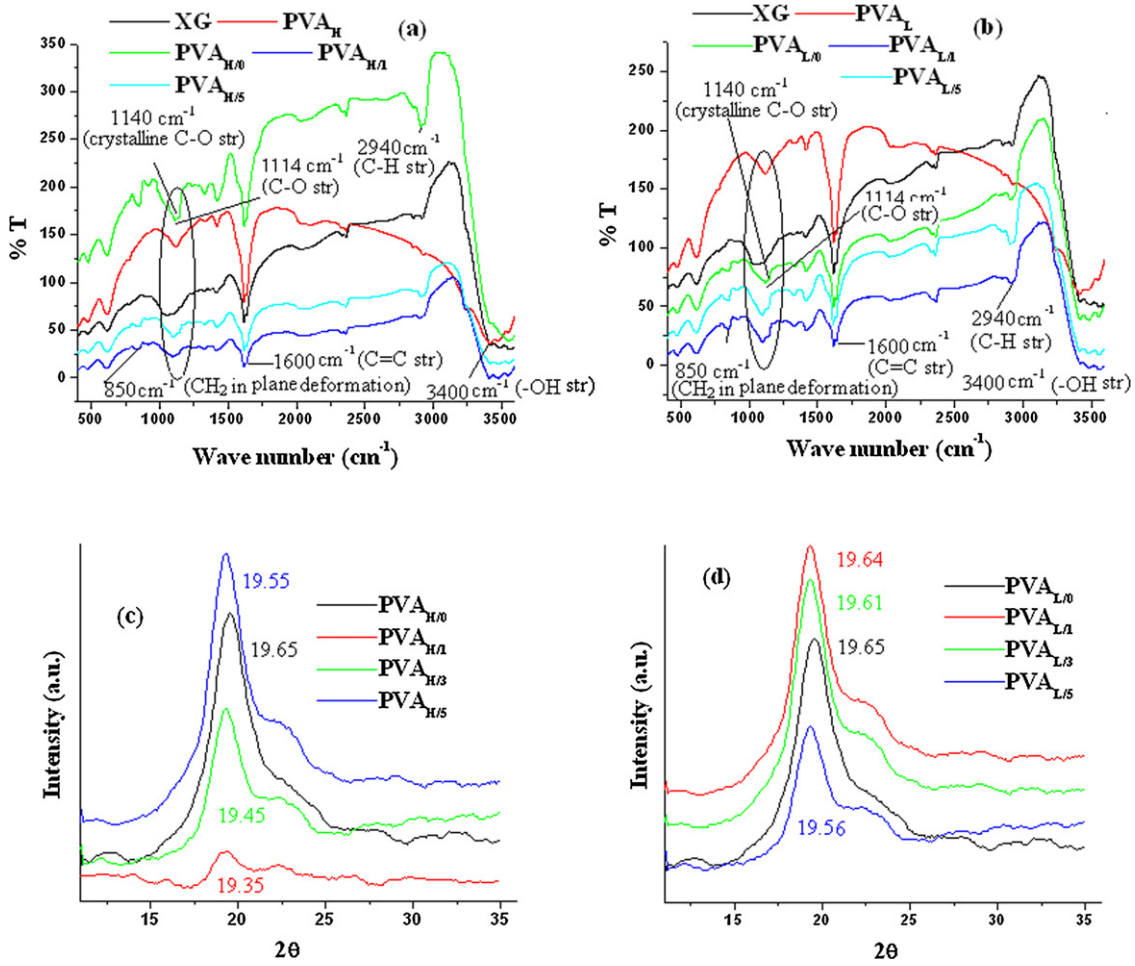

Fig. 2. (a and b) FTIR spectra and (c and d) dry state XRD patterns of neat PVAs and different PVA–XG hybrid membranes.

3. Results and discussion

3.1. Morphology analysis

AFM height and phase images of different irradiated membranes are displayed in Fig. 1. Presence of different phases results differences in surface adherence of the vibrating cantilever and dissipates variable amount of energy which produces different color. Normally highly dissipating domains are soft, amorphous and gray in color while less dissipating regions are bright and more crystalline in nature (Schon et al., 2011). The light gray domains indicate the mixed nature of them. The phase image of $PVA_{H/1}$ disclosed excellent fibrillar morphology of the harder phase (Fig. 1a). The average length of the fibers was 300 nm and average width was about 100 nm. The section analysis (Fig. 1b) showed highly undulated surface with average vertical distance of 7.49 nm. Those bulging features were dominantly the harder phase of the hybrid as seen through 3D imaging (Fig. 1c). But the scenario drastically changed on increasing XG content. The fibrillar morphology completely vanished and gross phase separation between hard and soft domains with very little interfacial adhesion became evident. The phase image of $PVA_{H/5}$ thus showed highly rough and wavy surface morphology (Fig. 1d). 3D image was complementary to that observation (Fig. 1e). It revealed that the crystalline lamella of nearly 1000 nm^2 surface area were preferably assembled on the surface while softer domains were mostly retained within the bulk. Conversely, $PVA_{L/5}$ elucidated (Fig. 1f and g) higher structural array of the harder phase in the topographical signal, similar to $PVA_{H/1}$ but hugely different from $PVA_{L/1}$ (Fig. 1i and j). In $PVA_{L/5}$, distinct fibrillar orientations of the harder domains were observed as opposed to aggregated crystal lamella in $PVA_{L/1}$. Section analysis (Fig. 1h) measured average vertical distance of those thinner fibrils as 18 nm which indicates presence of less undulated and more bulging surface features in $PVA_{L/5}$ than $PVA_{H/1}$. In $PVA_{L/1}$, the phase distinctions were not too great alike $PVA_{H/5}$.

Amazing contrast in phase miscibility between PVA_H and PVA_L with XG probably lies on the magnitude of viscosity differences among them with XG. Our earlier investigation showed PVA_L as surprisingly more viscous than PVA_H (Bhunia, Chattopadhyay, et al., 2011) despite of its extremely low molecular weight and that feature, in this case, had reduced viscosity differences between PVA_L and XG and produced better phase compatibility, particularly at higher XG content. On contrary, greater viscosity mismatches between PVA_H and XG, although had generated better phase mixing at low XG content, but had severely deteriorated and led to huge phase separation at high XG content. Infrared spectral analysis which provides microstructural evidence, could further enlighten this presumption in the following section.

3.2. Infrared spectroscopy analysis

The spectra show characteristic C—O stretching peak of XG at 1044 cm^{-1} in all blend compositions (Fig. 2a and b). The similar peak of PVA, originally appeared at 1112 cm^{-1}, was shifted in

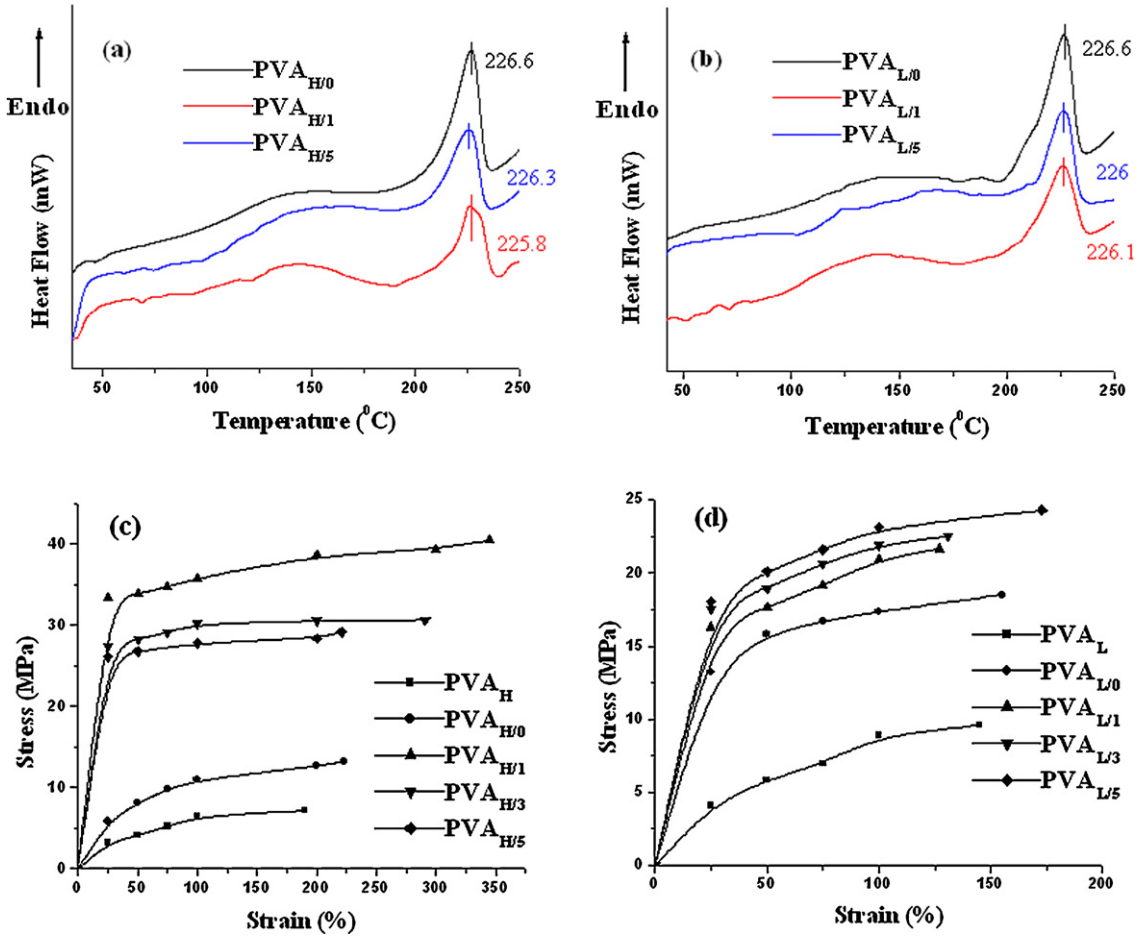

Fig. 3. (a and b) DSC curves and (c and d) dry state mechanical properties of neat PVAs and their hybrids.

irradiated hybrids to 1087, 1098, 1096 and 1085 cm^{-1} in PVA$_{H/1}$, PVA$_{H/5}$, PVA$_{L/1}$ and PVA$_{L/5}$ respectively. This low energy shift indicates hydrogen bonded interaction between primary and secondary alcohols of the blended components (Sudhamania, Prasad, & Udaya-Sankar, 2003). The interaction is evidently higher in PVA$_{H/1}$ and PVA$_{L/5}$ than in PVA$_{H/5}$ and PVA$_{L/1}$ (greater peak shift) and rightly proved our presumption on phase miscibility. A new peak, marking crystalline C—O stretching in neat PVA, appeared separately at 1140 cm^{-1} in all PVA-XG irradiated hybrids [Fig. 2a and b] (Bhunia et al., 2012; Lee, Lee, & Jang, 2008). This convicted presence of harder PVA fibrils but surprisingly as minor crystalline domains in post-irradiated hybrids despite of its higher original concentration (more than 90%). The crystallinity gradients were measured from the intensity ratio of the peaks at 1140 and 850 cm^{-1} (C—H bending) (Lee et al., 2008). The later (C—H bending peak of PVA) was taken as the standard since the particular band was expected to be least affected during irradiation. The results denoted in Table 1 show that 1 wt% XG content had induced maximum crystallinity in PVA$_H$ (PVA$_{H/1}$) whereas 5 wt% XG did the same in PVA$_L$ (PVA$_{L/5}$).

3.3. Wide angle X-ray (WAX) diffraction analysis

Evidence of PVA-crystallinity was further demonstrated from the moderately sharp diffraction peak near $2\theta = 19–20^\circ$ in Fig. 2 (Ricciardi, Auriemma, De-Rosa, & Laupretre, 2004). Fig. 2c shows those in PVA$_H$ series while Fig. 2d for PVA$_L$ series. The amorphous halo beyond the diffraction peak indicated amorphous XG phase (Arimura, Omagari, Yamamoto, & Kadokawa, 2011). Table 1 reports crystallite size, percent crystallinity and diffraction position of all irradiated hybrids, calculated from those figures. Crystallite sizes were determined using Scherrer equation described elsewhere (D'Agostino, 1992). Irradiated PVAs showed low crystallinity (touching to 4.1%) primarily due to radiation induced crosslinking of the dominant amorphous fraction. In, PVA$_H$, the crystallinity sharply reduced in presence of 1% XG. The diffraction peak angle also reduced and the crystallite size drastically increased from that of neat PVA$_H$. Rapid drop in crystallinity indicates huge loss of cohesive interaction courtesy establishment of higher PVA–XG interaction arranging PVA$_H$ segments into sharp crystalline fibrils, embedded within amorphous XG. But, gradual increase in XG content up to 5 wt% produced reverse phenomena i.e. increase in percent crystallinity and diffraction angle, while drop in crystallite size. The reason could be re-development of cohesive interaction due to PVA–XG viscosity mismatch. The trend however is just the reverse for PVA$_L$ hybrids as it implicates bigger crystallite formation despite marginal loss of cohesive interaction between PVA$_L$ segments (slight decrease of % crystallinity, Table 1). Neat PVA$_L$ usually produce more chain scission than crosslinking under electron beam irradiation than PVA$_H$ (Bhunia, Goswami, et al., 2011) which, perhaps, had been maximally prevented in presence of XG otherwise, the crystallinity loss would have been much greater than what actually has been recorded. Close viscosity match with XG produced better phase mixing and interaction which prevented phase separation and degradation of PVA$_L$ molecules on a large scale. It further helped in morphological transformation from smaller crystalline lamella to bigger crystalline fibrils at higher XG content.

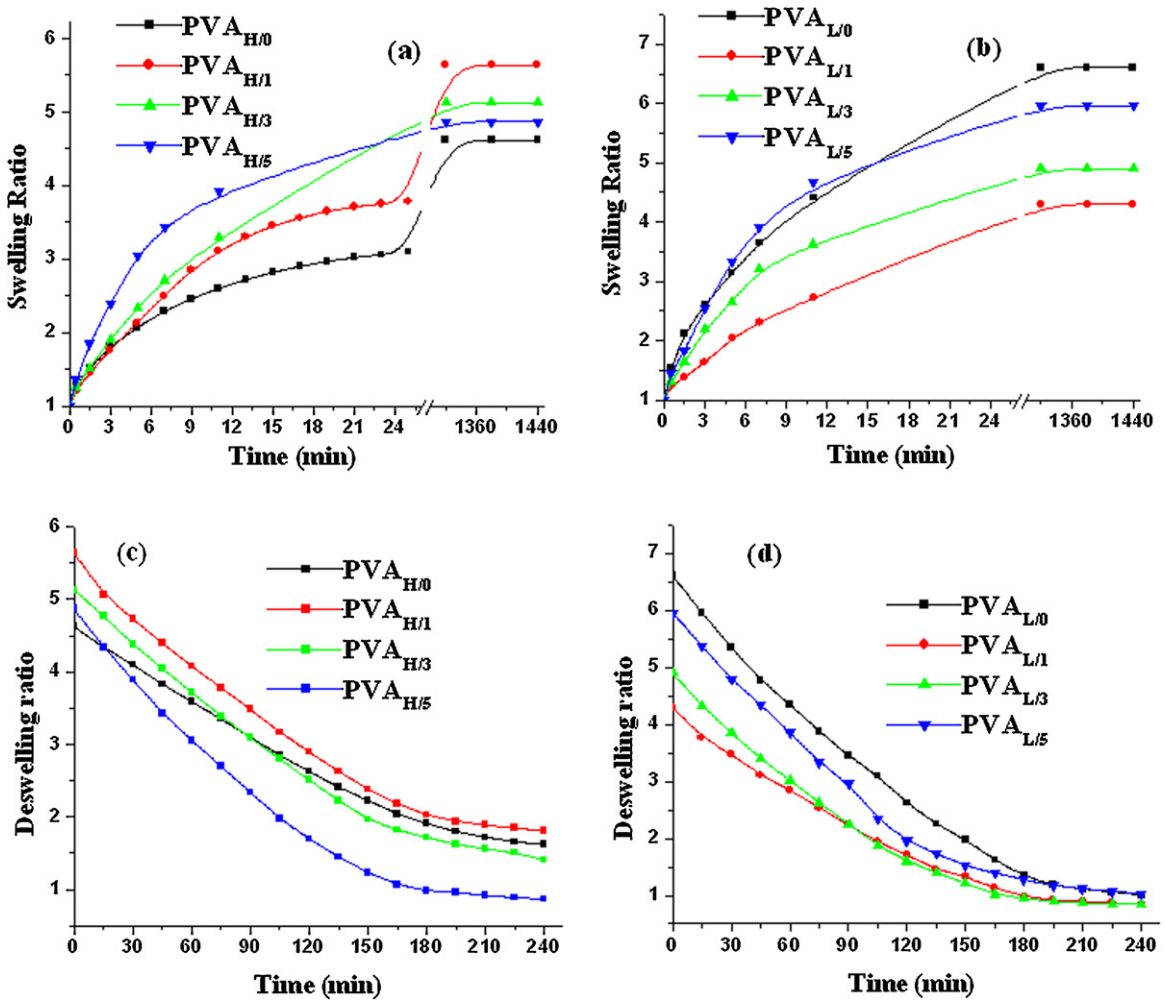

Fig. 4. Hydroswelling and de-swelling kinetics of different PVA–XG hybrid membranes.

3.4. Thermal analysis

Since hybrids with 1 and 5 wt% XG contents gave interesting variation, DSC traces of them were taken and analyzed (Fig. 3a and b). Neat PVAs usually show sharp crystalline melting at 227 °C preceded by a weak endotherm between 130 and 160 °C revealing interaction between their amorphous and crystalline domains (Layek, Samanta, & Nandi, 2012). The irradiated PVAs, in this case, have shown the crystalline melting peak at 226.6 °C, due to low percentage crystallinity. The melting peak in $PVA_{H/1}$ was further preponed (225.8 °C) due to further crystallinity loss in presence of XG. But in $PVA_{L/1}$, it was more close to the original sample (226.1 °C) since it recorded less crystallinity loss at similar XG content. Even in $PVA_{L/5}$, which produced maximum loss in crystallinity, the melting occurs at 226 °C. The drop in PVA crystallinity upon addition of XG was equivalent to the rise in adhesive interaction between them (Sudhamania et al., 2003) demonstrated through drop in melting enthalpy at each composition (reduction in melting peak area). The values are reported in Table 1. The trend excellently corroborates net crystallinity data calculated from X-ray diffraction analysis. $PVA_{H/1}$ had much lower melting enthalpy than $PVA_{H/5}$ while in PVA_L series it was $PVA_{L/5}$ which recorded the lowest melting enthalpy leading to highest crystallinity loss in the respective series due to strong adhesive interaction.

3.5. Analysis of mechanical properties

The tensile property trends are interesting (Fig. 3c and d). Unirradiated PVAs were weaker. The tensile strength was 6 MPa for PVA_H and 9 MPa for PVA_L. PVA_L had shown slightly greater strength due to its higher viscosity than PVA_H (Bhunia, Chattopadhyay, et al., 2011). On irradiation, the tensile strength rose to 13 MPa in $PVA_{H/0}$ whereas it had further increased to 17.5 MPa in $PVA_{L/0}$. Tensile modulus had also drastically improved in $PVA_{L/0}$ than that in $PVA_{H/0}$ but net elongation followed the reverse trend. Both tensile strength and modulus became higher in the irradiated membranes due to crosslinking and net rise in percent crystallinity (Bhunia et al., 2012). But it was much interesting to note higher improvement in $PVA_{L/0}$ than in $PVA_{H/0}$ despite of its greater chain degradation tendency than crosslinking (Bhunia, Goswami, et al., 2011). Presence of XG in the hybrids had radically improved tensile modulus, strength and elongation in PVA_H whereas it was comparatively much less in PVA_L. $PVA_{H/1}$ had displayed maximum tensile modulus, strength and elongation due to presence of strong fibrillar PVA. In $PVA_{H/3}$ and $PVA_{H/5}$, lamellar PVA does not impart such reinforcement for which the strength and elongation had reduced significantly. Similarly, fibrillar PVA maximally reinforced $PVA_{L/5}$ by showing highest strength and elongation values among all PVA_L hybrids but then gradually decreased owing to formation of lamellar PVA crystallites at other compositions.

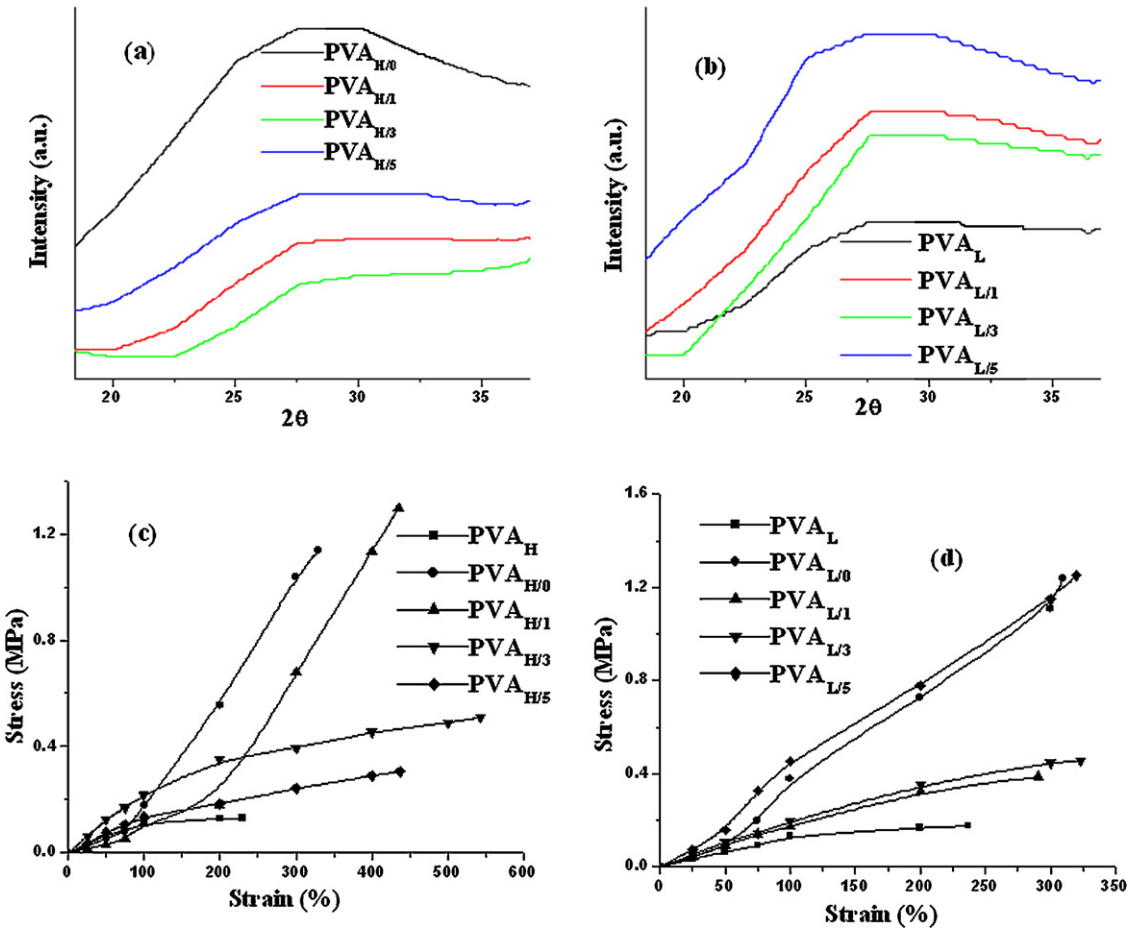

Fig. 5. Wet state XRD (a and b) and mechanical properties (c and d) of different PVA–XG hybrids.

3.6. Analysis of hydroswelling and de-swelling kinetics

Hydroswelling kinetics of irradiated PVA_H, PVA_L and all their hybrid membranes are shown in Fig. 4a and b. It is demonstrated that irradiated $PVA_{L/0}$ swelled much faster than $PVA_{H/0}$ and absorbed significantly high amount of water due to presence of shorter and more flexible degraded chain fragement which allows faster water intake (Bhunia, Chattopadhyay, et al., 2011). In blends, it was interesting to note that despite gradual rise in swelling rate with increasing XG content in PVA_H, the net swelling ratio eventually followed the reverse trend (Fig. 4a). In PVA_L, both swelling rate and ratio, after a drastic drop on addition of 1 wt% XG ($PVA_{L/1}$), had eventually increased significantly in $PVA_{L/3}$ and $PVA_{L/5}$ with $PVA_{L/5}$ nearly shown equivalent swelling profile alike $PVA_{L/0}$ especially at the initial stage (Fig. 4b). Drop in swelling rate could well be due to crosslinking and high interfacial interaction produced on irradiation. It was better manifested in $PVA_{L/1}$ and $PVA_{L/3}$ ($PVA_{L/1} > PVA_{L/3}$) since lamellar PVA_L and amorphous XG were nearly co-continuous. In $PVA_{L/5}$, the effect of crosslinking was evidently less perhaps due to more hygroscopic XG content at the surface which catalyzed faster water absorption. In PVA_H, the effect was even lower in all hybrid membranes than PVA_L probably due to low phase mixing and interfacial interaction. They although had allowed hygroscopic XG for faster water absorption as its content in the hybrid was increased, but eventually led to low water uptake following the ascending order in $PVA_{H/1} > PVA_{H/3} > PVA_{H/5}$.

Fully swollen hybrids on standing spontaneously release water to dissipate the impressed stress on swelling. It is usually seen that hybrids absorbing higher amount of water i.e. having high net swelling ratio releases more water than those which previously had shown lower water intake (Bhunia, Goswami, et al., 2011). It is aptly followed in $PVA_{L/5}$ and $PVA_{L/0}$ in PVA_L series and $PVA_{H/5}$ in PVA_H series. Apart from these, the de-swelling rate was highly competitive. Equilibrium water content was always higher in all PVA_H hybrids than those in PVA_L series, except $PVA_{H/5}$. It was due to more hydroxyl content in PVA_H than in PVA_L which hold higher equilibrium water than PVA_L hybrids.

3.7. Swelled state X-ray diffraction and mechanical property analysis

Swelled-state diffractograms of the hybrids in Fig. 5a and b elucidates complete abolition of PVA crystallinity. Both lamellar and fibrillar PVA crystals became amorphous on extensive water intake. The amorphous halo of the XG phase also had widened due to its large volume increment. Swelled state mechanical properties are displayed in Fig. 5c and d. The membrane turned weaker (tensile modulus and strength) but became highly extensible. Drop in strength was due to loss in PVA crystallinity while higher elongation was due to plasticization induced by large volume of water trapped inside the crosslinked network. But it was noted that PVA_H hybrids suffered lower property loss than PVA_L hybrids on swelling. $PVA_{H/0}$ and $PVA_{H/1}$ in PVA_H series and $PVA_{L/0}$ and $PVA_{L/5}$ in PVA_L series had interestingly displayed rubber like deformation equivalent to stress-induced crystallization phenomenon. Highly swelled crosslinks in neat PVAs and the swollen PVA fibrils in the crosslinked hybrids ($PVA_{H/1}$ and $PVA_{H/5}$) were perhaps responsible for this behavior in the swollen state.

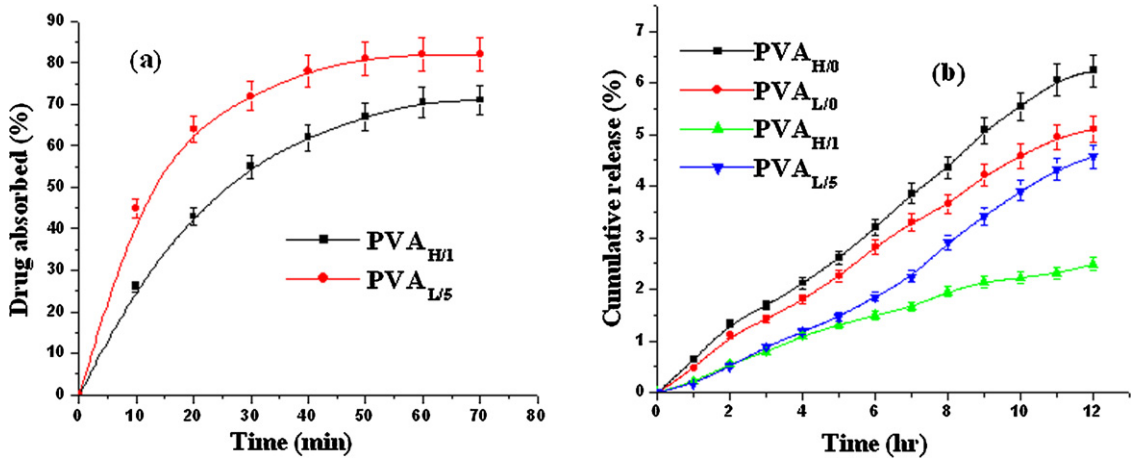

Fig. 6. (a) DEE of PVA$_{H/1}$ and PVA$_{L/5}$ and (b) cumulative (%) release of diltiazem from PVA$_{H/0}$, PVA$_{L/0}$, PVA$_{H/1}$ and PVA$_{L/5}$ membranes.

3.8. DEE analysis

Fig. 6a compares DEE between most physico-mechanically balanced PVA$_{H/1}$ and PVA$_{L/5}$ membranes for diltiazem encapsulation and release analysis. Drug encapsulation by PVA$_{L/5}$ was clearly much higher than PVA$_{H/1}$, perhaps due to favorable retention vs. elution equilibrium induced by the former despite of its greater swelling character than PVA$_{H/1}$. The data shows, within first 10 min, 45% of the drug was absorbed by PVA$_{L/5}$ whereas only 26% by PVA$_{H/1}$ and finally the saturation achieved within 50 min in PVA$_{L/5}$ while in 60 min in PVA$_{H/1}$. PVA$_{L/5}$ showed better phase mixing between PVA$_L$ which probably excelled drug-polymer interaction. In PVA$_{H/1}$, the diltiazem molecules were mostly distributed among PVA and XG, which, because of their different phase viscosity, could not produce strong drug retention alike PVA$_{L/5}$.

3.9. Diltiazem release kinetics study

Fig. 6b shows cumulative release (%) of diltiazem from PVA$_{H/1}$ and PVA$_{L/5}$ membranes fitted in a Franz diffusion cell. Data on

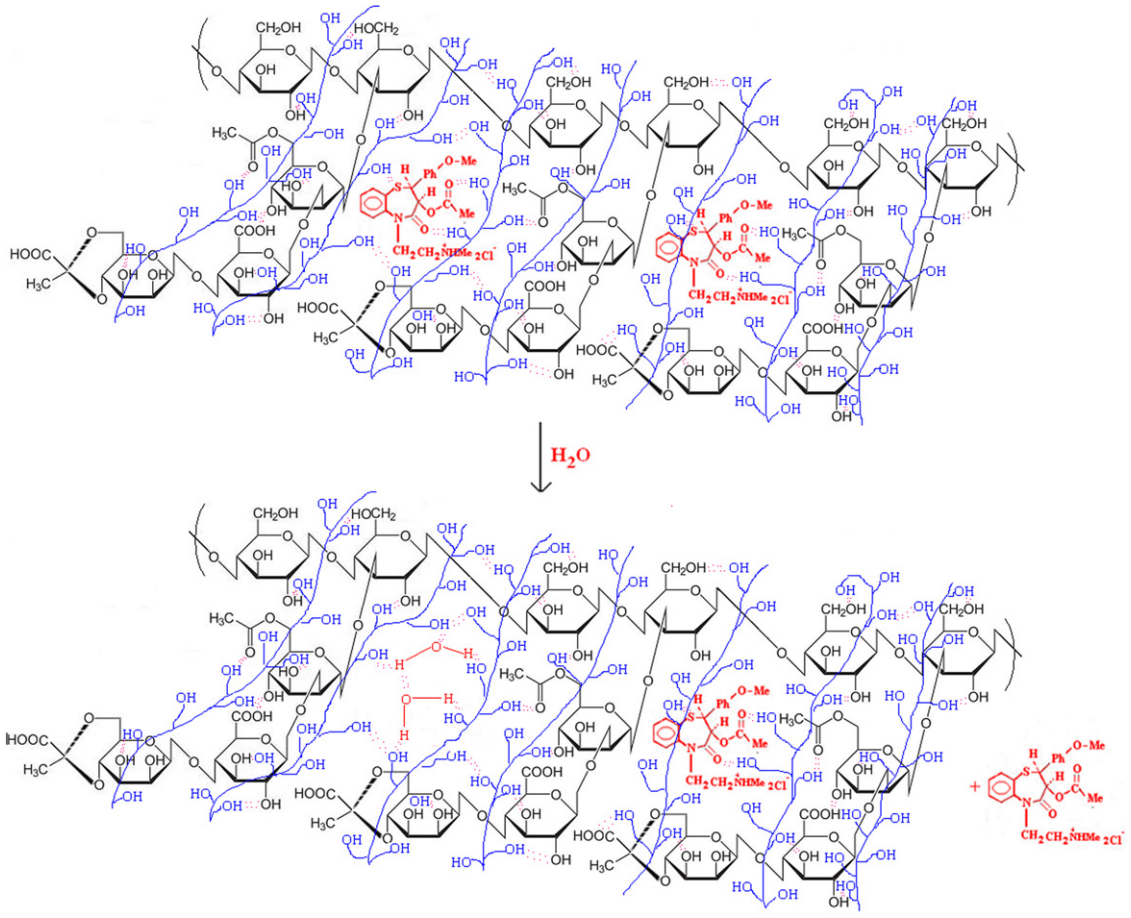

Fig. 7. A schematic showing diltiazem encapsulation within irradiated fibrillar PVA–XG matrix and its subsequent release under swelled state.

$PVA_{H/0}$ and $PVA_{L/0}$ were also included to understand the variation. The release was monitored for 12 h and the time dependent release data were fitted into the most prevalent power law model stated in Eq. (1) (Bhunia, Chattopadhyay, et al., 2011; Peppas, Bures, Leobandung, & Ichikawa, 2000)

$$\frac{M_t}{M_\alpha} = k \cdot t^n \quad (1)$$

where M_t/M_α denotes fractional release of diltiazem at time 't'. 'k' and 'n' are constants related to diffusion coefficient and specific drug transport mechanism. The 'k' and 'n' values are reported in Table 1. Our earlier investigation showed sharp bursting features of PVA_H and PVA_L which completely disappeared in $PVA_{H/0}$ and $PVA_{L/0}$ after irradiation. But precise control over diltiazem elution was still not achieved, as the exponents were 0.91 and 0.92. $n \geq 0.5$ indicates case II transport which follows a mixed mechanism of Fickian and non-Fickian type and is difficult to control (Peppas & Khare, 1995). However, $n \geq 1$, observed for both $PVA_{H/1}$ (1.21) and $PVA_{L/5}$ (1.11), fully stands for relaxation controlled release having better control than case II transport. But $n \approx 1$ obtained for $PVA_{H/1}$ ensured even better control over the diltiazem release than $PVA_{L/5}$. It was interesting to observe such contrasting behavior of $PVA_{H/1}$ despite of its lower DEE than $PVA_{L/5}$. The probable reason could be (i) its higher equilibrium water content and (ii) stronger post-swelled mechanical properties than $PVA_{L/5}$. Entrapment of diltiazem within PVA–XG hybrid was a function of drug–PVA–XG interaction through hydrogen bonding (Fig. 7). Since the release is fully relaxation based it primarily depends on segmental flexibility of the polymers in the swelled state, which evidently was less in $PVA_{H/1}$ than in $PVA_{L/5}$ due to higher modulus and strength. High flexibility in $PVA_{L/5}$ thus allowed more diltiazem to elute in swelled state even though it had shown higher DEE than $PVA_{H/1}$. Overall release was 2.5% from $PVA_{H/1}$ and 4.6% from $PVA_{L/5}$ after 12 h observation.

4. Conclusion

High viscosity of XG has turned down PVA into minor phase despite of its very higher concentration in irradiated PVA–XG blends. Both PVA_H and PVA_L were crystalline but the structure drastically altered with XG concentration and its viscosity differences with PVA_H and PVA_L. Thinner PVA fibrils in $PVA_{L/5}$ arosed higher diltiazem encapsulation due to stronger interaction than its slightly thicker orientation in $PVA_{H/1}$ but the elution was more sustained and slow from the later due to greater segmental stiffness under swelled condition. But the amount of release obtained from both $PVA_{H/1}$ and $PVA_{L/5}$ probably suggests use of multiple patches for therapy in future experiments and trials.

References

Arimura, T., Omagari, Y., Yamamoto, K., & Kadokawa, J. (2011). Chemoenzymatic synthesis and hydrogelation of amylose-grafted xanthan gums. *International Journal of Biological Macromolecules*, *49*, 498–503.

Barash, H. E., Orbey, G., Polat, B. E., Ewoldt, R. H., Feshitan, J., Langer, R., et al. (2010). A microcomposite hydrogel for repeated on-demand ultrasound-triggered drug delivery. *Biomaterials*, *31*, 5208–5217.

Bhunia, T., Bhowmik, M., Chattopadhyay, D., & Bandyopadhyay, A. (2012). Interesting correlation between structure, physicomechanical, swelling and sustained transdermal release behavior of diltiazem hydrochloride in various poly(vinyl alcohol) hydrogel membranes. *Journal of Applied Polymer Science*, *124*, E177–E189.

Bhunia, T., Chattopadhyay, D., & Bandyopadhyay, A. (2011). Gel viscosity influenced by nanosilica phase morphology in high and low molecular weights PVA-ex-situ silica hybrids. *Journal of Sol–Gel Science and Technology*, *59*, 260–268.

Bhunia, T., Goswami, L., Chattopadhyay, D., & Bandyopadhyay, A. (2011). Sustained transdermal release of diltiazem hydrochloride through electron beam irradiated different PVA hydrogel membranes. *Nuclear Instruments and Method in Physics Research B*, *269*, 1822–1828.

Bhunia, T., Giri, A., Nasim, T., Chattopadhyay, D., & Bandyopadhyay, A. (2013). A transdermal diltiazem hydrochloride delivery device using multi-walled carbon nanotube/poly (vinyl alcohol) composites. *Carbon*, *52*, 305–315.

Chandra, R., & Rustgi, R. (1998). Biodegradable polymers. *Progress in Polymer Science*, *23*, 1273–1335.

Coombes, A. G. A., & Meikle, M. C. (1994). Resorbable synthetic polymers s replacements for bone graft. *Clinical Materials*, *17*, 35–67.

D'Agostino, A. T. (1992). Determination of thin metal film thickness by X-ray diffractometry using the Scherrer equation, atomic absorption analysis and transmission/reflection visible spectroscopy. *Analytica Chimica Acta*, *262*, 269–275.

Davaran, S., Rashidi, M. R., Khandaghi, R., & Hashemi, M. (2005). Development of a novel prolonged-release nicotine transdermal patch. *Pharmacological Research*, *51*, 233–237.

Deng, L., & Hagg, M. B. (2010). Swelling behavior and gas permeation performance of PVAm/PVA blend FSC membrane. *Journal of Membrane Science*, *363*, 295–301.

Finch, C. A. (1973). *Poly (vinyl alcohol)—Properties and application* (1st ed.). London: John Wiley and Sons, Ltd.

Gao, Y., Liang, J., Liu, J., & Xiao, Y. (2009). Double-layer weekly sustained release transdermal patch containing gestodene and ethinylestradiol. *International Journal of Pharmaceutics*, *377*, 128–134.

Garcia-Ochoa, F., santos, V. E., Casas, J. A., & Gomez, E. (2000). Xanthan gum: Production, recovery and properties. *Biotechnology Advances*, *18*, 549–579.

Huang, R., Qi, W., feng, L., Su, R., & He, Z. (2011). Self-assembling peptide-polysaccharide hybrid hydrogel as a potential carrier for drug delivery. *Soft Matter*, *7*, 6222–6230.

Izawa, H., Kaneko, Y., & Kadokawa, J. (2009). Unique gel of xanthan gum with ionic liquid and its conversion into high performance hydrogel. *Journal of Matererial Chemistry*, *19*, 6969–6972.

Jiang, S., Liu, S., & Feng, W. (2011). PVA hydrogel properties for biomedical application. *Journal of Mechanical Behavior of Biomedical Materials*, *4*, 1228–1233.

Kotiyan, P. N., Vavia, P. R., Bharadwaj, Y. K., Sabarwal, S., & Majali, A. B. (2002). Electron beam processed transdermal delivery system for administration of an anti-anginal agent. *Radiation Physics and Chemistry*, *65*, 641–646.

Layek, R. K., Samanta, S., & Nandi, A. K. (2012). The physical properties of sulfonated graphene/poly(vinyl alcohol) composites. *Carbon*, *50*, 815–827.

Lee, J., Lee, K. J., & Jang, J. (2008). Effect of silica nanofillers on isothermal crystallization of poly(vinyl alcohol): In-situ ATR-FTIR study. *Polymer Testing*, *27*, 360–367.

Lee, Y. M., Kim, S. H., & Kim, S. J. (1996). Preparation and characteristics of β-chitin and poly (vinyl alcohol) blend. *Polymer*, *37*, 5897–5905.

Mahmarian, J. J., Fenimore, N. L., Marks, G. F., Francis, M. J., Ballejo, H. M., Verani, M. S., et al. (1994). Transdermal nitroglycerin patch therapy reduces the extent of exercise-induced myocardial ischemia: results of a double-blind, placebo-controlled trial using quantitative thallium-201 tomography. *Journal of American College of Cardiology*, *24*, 25–32.

Middleton, J. C., & Tipton, A. J. (2000). Synthetic biodegradable polymers as orthopedic devices. *Biomaterials*, *21*, 2335–2346.

Nishino, T., Kani, S. C., Gotoh, K., & Nakamae, K. (2002). Melt processing of poly(vinyl alcohol) through blending with sugar pendant polymer. *Polymer*, *43*, 2869–2873.

Nuttelman, C. R., Henry, S. M., & Anseth, K. S. (2002). Synthesis and characterization of photocrosslinkable, degradable poly (vinyl alcohol) based tissue engineering scaffolds. *Biomaterials*, *23*, 3617–3626.

Pakhomov, P. M., Korsukov, V., Shablygin, Ye., & Novak, M. V. I. I. (1984). Relation between mechanical properties and conformational composition of polymers. *Polymer Science USSR*, *26*, 1441–1447.

Peppas, N. A., Bures, P., Leobandung, W., & Ichikawa, H. (2000). Hydrogels in pharmaceutical formulations. *European Journal of Pharmaceutics and Biopharmaceutics*, *50*, 27–46.

Peppas, N. A., & Khare, A. R. (1995). Swellig/deswelling of anionic copolymer gels. *Biomaterials*, *16*, 559–567.

Peterson, R. C., Wolffsohn, J. S., Nick, J., Winterton, L., & Lally, J. (2006). Clinical performance of daily disposable soft contact lenses using sustained release technology. *Contact Lens & Anterior Eye*, *29*, 127–134.

Prisant, L. M., & Elliott, W. J. (2003). Drug delivery systems for treatment of systemic hypertension. *Clinical Pharmacokinetics*, *44*, 931–940.

Puche, J. J., Garcia-Coret, M. J., Villalba, F. L., Mahmoud, I. A., & Roig, J. V. (2010). Local treatment of a chronic anal fissure with diltiazem vs. nitroglycerin. A comparative study. *Cirugia Espanola (English Edition)*, *87*, 224–230.

Raynaud, J. P., Aumonier, C., Gualano, V., Betea, D., & Beckers, A. (2008). Pharmacokinetic study of a new testosterone-in-adhesive matrix patch applied every 2 days to hypogonadal men. *The Journal of Steroid Biochemistry and Molecular Biology*, *109*, 177–184.

Ricciardi, R., Auriemma, F., De-Rosa, C., & Laupretre, F. (2004). X-ray diffraction analysis of poly(vinyl alcohol) hydrogels, obtained by freezing and thawing techniques. *Macromolecules*, *37*, 1921–1927.

Schon, P., Bagdi, K., Molnar, K., Markus, P., Pukanszky, B., & Vancso, G. J. (2011). Quantitative mapping of elastic moduli at the nanoscale in phase separated polyurethanes by AFM. *European Polymer Journal*, *47*, 692–698.

Sereno, N. M., Hill, S. E., & Mitchell, J. R. (2007). Impact of the extrusion process on xanthan gum behavior. *Carbohydrate Research*, *342*, 1333–1342.

Singh, B., & Sharma, V. (2010). Design of psyllium–PVA–acrylic acid based novel hydrogels for use in antibiotic drug delivery. *International Journal of Pharmaceutics*, *389*, 94–106.

Stammen, J. A., Williams, S., Ku, D. N., & Guldberg, R. E. (2001). Mechanical properties of a novel PVA hydrogel in shear and unconfined compression. *Biomaterials*, *22*, 799–806.

Sudhamania, S. R., Prasad, M. S., & Udaya-Sankar, K. (2003). DSC and FTIR studies on gellan and polyvinyl alcohol (PVA) blend films. *Food Hydrocolloids*, *17*, *245*–250.
Tang, Q., Sun, X., Li, Q., Wu, J., & Lin, J. (2009). Fabrication of a high-strength hydrogel with an interpenetrating network structure. *Colloids and Surface A: Physicochemical Engeneering Aspects*, *346*, 91–98.
Tanzi, M. C., Barozzi, C., Tieghi, Q., Ferrara, R., Casini, G., & Tempesti, F. (1985). Heparinizable graft copolymers from chlorosulphonated polyethylene with poly(amido-amine) segments. *Biomaterials*, *6*, 273–276.
Wang, X. L., Oh, I. I.-K., & Lee, S. (2010). Electroactive artificial muscle based on crosslinked PVA/SPTES. *Sensors and Actuators B: Chemical*, *150*, 57–64.
Xiao, C., & Zhou, G. (2003). Synthesis and properties of degradable poly (vinyl alcohol) hydrogel. *Polymer Degradation and Stability*, *81*, 297–301.
Yang, W. H., Smolen, V. F., & Peppas, N. A. (1981). Oxygen permeability coefficients of polymers for hard and soft contact lens applications. *Journal of Membrane Science*, *9*, 53–67.
Yoon, S. D., Park, M. H., & Byun, H. S. (2012). Mechanical and water barrier properties of starch/PVA composite films by adding nano-sized poly(methyl methacrylate-co-acrylamide) particles. *Carbohydrate Polymers*, *87*, 676–686.
Zhang, J., Yuan, K., & Wang, W. P. (2007). Preparation and pH responsive behavior of poly (vinyl alcohol)- chitosan- poly (acrylic acid) full-IPN hydrogels. *Journal of Bioactive and Compatible Polymers*, *22*, 207–218.
Zhao, L., Mitomo, H., Zhai, M., Yoshii, F., Nagasawa, N., & Kume, T. (2003). Synthesis of antibacterial PVA/CM-chitosan blend hydrogels with electron beam irradiation. *Carbohydrate Polymers*, *53*, 439–446.